# Atomic layer deposition of energy band tunable tin germanium oxide electron transport layer for the SnS-based solar cells with 400 mV open-circuit voltage

# Atomic Layer Deposition of Energy Band Tunable Tin Germanium Oxide Electron Transport Layer for the SnS-based Solar Cells with 400 mV Open-circuit Voltage

Danny Chua[1], Sang Bok Kim[1], Prasert Sinsermsuksakul[1], and Roy Gordon[1*]
[1] *Harvard University, Cambridge, MA 02138, USA*
[*] *Corresponding author: gordon@chemistry.harvard.edu*

Tin germanium oxide, $(Sn,Ge)O_2$, films were prepared using atomic layer deposition and tailored to SnS absorber layer by incorporating various amounts of germanium into tin oxide to adjust band alignments at the interfaces of SnS/$(Sn,Ge)O_2$ photovoltaic devices. Carrier concentrations of $(Sn,Ge)O_2$ were suppressed from $10^{20}$ to $10^{18}$ $cm^{-3}$ with germanium incorporation, with nitrogen doping of further reducing carrier concentrations by another order of magnitude. Excellent tunability of both band energy levels and carrier concentrations of $(Sn,Ge)O_2$ allowed optimizing SnS-based solar cells. SnS/$(Sn,Ge)O_2$:N devices were demonstrated, with an open-circuit voltage as high as 400 mV, due to effective mitigation of interfacial recombination of photogenerated carriers at the SnS/$(Sn,Ge)O_2$:N absorber-buffer heterojunction interface.

Tin monosulfide (SnS) is a promising earth abundant and non-toxic p-type semiconductor material for photovoltaic applications. SnS thin films have displayed many desirable properties including a suitable bandgap of 1.1 eV, high absorption coefficients exceeding $10^{14}$ $cm^{-1}$ and sufficiently high mobilities ($\mu$ ~ 10 $cm^2V^{-1}s^{-1}$), making it an attractive alternative to leading thin film absorber materials[1-5]. The better performing SnS-based devices utilize a tunable n-type buffer layer to optimize the conduction band offset (CBO) at the p-n junction interface. Therefore, tuning the conduction band energy level of the n-type buffer is critical for enabling efficient collection of photogenerated carriers. A "spike" structure is formed when the conduction band edge of the p-type absorber layer is lower than that of the n-type buffer layer ($E_{c,absorber} < E_{c,buffer}$) forming a barrier that impedes the collection of photogenerated carriers. Theoretical studies have predicted the optimal offsets to reside in the range between 0 eV and +0.4 eV[6]. On the other hand, a "cliff" structure ($E_{c,absorber} > E_{c,buffer}$) increases charge recombination at the interface of a p-type absorber and n-type buffer[6, 7].

The best performing SnS solar cells with device efficiencies of 4.63 % were achieved using a p-SnS/n-$SnO_2$/n-Zn(O,S):N structure where Zn(O,S):N serves the role of the n-type buffer layer whose energy band levels can be tuned with varying compositions of O and S. Interfacial recombination can be suppressed by optimizing the heterojunction interface to have a small "spike" structure[8, 9]. The insertion of an ultra-thin $SnO_2$ ALD layer between the SnS and Zn(O,S):N layers was later discovered to significantly increase the open-circuit voltage ($V_{OC}$)[10]. It is believed that the $SnO_2$ acts as a diffusion layer that prevent the zinc diffusion into SnS during the Zn(O,S):N ALD process, resulting in increased recombination at the p-n interface and hence in the loss of the junction's rectification properties. While a few monolayers of $SnO_2$ produced the highest device performance, the device suffered performance degradation when the oxide layer thickness is thick enough to form a conduction band. This can be explained by the unfavorable cliff structure of the SnS/$SnO_2$ junction disrupting the optimized spike structure formed at the SnS/Zn(O,S):N interface. Consequently, a small spike structure at the interface not only reduced charge recombination at the interface but also avoided impeding the efficient collection of the photo-generated carriers with a sufficiently low barrier height at this interface.

Germanium-doped tin oxide is a logical advancement towards the design of an improved n-type buffer layer for SnS-based solar cell devices. This buffer layer material delivers two distinct advantages. First, there will be no potential diffusion of Zn like in the case of Zn(O,S):N. By replacing the Zn-based buffer layer, with a tin-based material, we eliminate the problem of detrimental deep-level defects in SnS arising from zinc diffusing out of the buffer layer into the SnS absorber. Secondly, replacing the corrosive and toxic co-reactant $H_2S$ with a non-corrosive organometallic ALD precursor for germanium enables greater control over the doping levels for finer CBO adjustments. Theoretical calculations also show the passivating effects that an oxide layer has on the surfaces of SnS where dangling bonds exist[11]. The optimal CBOs provided by an optimized Zn(O,S) layer is similarly achievable through fine-tuning the conduction band edges of $SnO_2$ by doping germanium into tin oxide, transforming the original cliff structure to a desired spike structure predominantly by raising the conduction band energy level. Therefore, to create the desired spike structure at the heterojunction interface, fine-tuning of composition is indispensable.

This work presents SnS-based photovoltaic devices using $(Sn,Ge)O_2$ as an n-type buffer layer. By leveraging the tunability of band alignments and adjustability of carrier densities, $(Sn,Ge)O_2$ is found to be a promising n-type buffer layer suitable for not only SnS, but also highly applicable to various p-type absorber materials, such as $Cu(In,Ga)(S,Se)_2$ (CIGS)[12, 13] and $Cu_2ZnSn(Se,S)_4$ (CZTS)[14-16]. ALD as the fabrication technique of choice for $(Sn,Ge)O_2$ provides precise control over the doping levels of Ge and N simply by adjusting the ratio of precursor pulses. The effects of germanium and nitrogen doping on the CBO and the conductivity of the materials were determined to guide this optimization.

An ALD process was used to deposit $SnO_2$ using tetrakis(dimethylamido)tin(IV) ($[(CH_3)_2N]_4Sn$, TDMASn, Sigma Aldrich) and hydrogen peroxide ($H_2O_2$, 30 % w/w in $H_2O$, Sigma Aldrich). Vapors of TDMASn and $H_2O_2$ were injected sequentially into the deposition

chamber. To prepare $(Sn,Ge)O_2$, germanium was doped into $SnO_2$ by injecting vapors of germanium(IV) methoxide ($Ge(OCH_3)_4$, Sigma Aldrich) and $H_2O_2$. TDMASn, $Ge(OCH_3)_4$ and $H_2O_2$ were kept at 60 °C, 30 °C and 30 °C, respectively. Thermally oxidized silicon wafers, glassy carbon plates, and silica glass were utilized as substrates and were treated by a UV/ozone cleaner (wavelengths = 185 nm and 254 nm) for 5 minutes at room temperature before being introduced into the process chamber. The band alignments at the $SnS/SnGeO_2$ interface were determined by x-ray photoelectron spectroscopy (XPS, Thermo Scientific K-alpha XPS) films using bilayered films of SnS with $(Sn,Ge)O_2$ overlayers [17]. The transmittance and reflectance spectra of 500-nm-thick SnS and 100-nm-thick $(Sn,Ge)O_2$ were measured at normal incidence with ultraviolet/visible and near-infra-red spectrophotometry (Hitachi U-4100 UV-vis-NIR spectrophotometer) in the wavelength range of 200 to 800 nm. Film thicknesses were measured using x-ray reflectivity (PANalytical X-Pert Pro) and cross-section scanning electron microscopy (Carl Zeiss Ultra 55 FESEM).

A photovoltaic device structure of $Si/SiO_2/Mo/SnS/(Sn,Ge)O_2/ZnO/ITO/Ag$ was used in this study. A Mo bilayer[18] was first sputtered on silicon (100) substrates with 300 nm thick layers of thermally oxidized silicon dioxide on the surface. 500-nm-thick SnS thin film absorber layers were deposited at 120 °C using an ALD of bis(*N, N'* - diisopropylformamidinato)Sn(II) ($Sn(famd)_2$, Strem Chemicals) and hydrogen sulfide ($H_2S$, 4 % in $N_2$) maintained at 60 °C and 25 °C, respectively. The SnS films were then annealed under a constant flow of 60 sccm of $H_2S$ at 400 °C and 10 Torr pressure for an hour. ZnO thin film was deposited at 120 °C by ALD using alternating doses of diethylzinc ($Zn(C_2H_5)_2$, DEZ, Sigma Aldrich) and deionized water vapor. 300 nm of tin-doped indium oxide (ITO) was deposited at room temperature via RF magnetron sputtering with a shadow mask to define an active device area of 0.24 $cm^2$. A 500-nm-thick Ag layer acting as the top electrode was patterned by e-beam evaporation using another shadow mask at room temperature.

$(Sn,Ge)O_2$ thin films were prepared at a substrate temperature of 200 °C which is within the common temperature windows for the ALD processes of $SnO_2$ and $GeO_2$. Tin oxide films have been deposited by ALD in the process temperatures of 50-300 °C using TDMA(Sn) as the tin source[19]. $Ge(OCH_3)_4$ was discovered to not deposit a $GeO_2$ film on non-hydroxylated surfaces at substrate temperatures of 200-300 °C. Instead, the precursor required the OH-terminated surfaces of ALD-$SnO_2$ and temperatures of at least 200 °C for the reaction with water vapor to occur and promote the incorporation of germanium into $SnO_2$. The lower end of the overlapping ALD temperature window of 200 °C was selected to exploit the reduced doping efficiency of germanium, allowing us to establish finer control over film compositions and access more uniform distribution of dopants throughout the film.

**Figure S1** shows the germanium content in the $(Sn,Ge)O_2$ film is approximately equal to the precursor pulse ratio, indicating excellent doping efficiency of Ge in the presence of OH-terminated surfaces during the Ge precursor pulse, and slightly more so in films with greater amount of Ge incorporated. Carbon and nitrogen peaks were observed only on the surface of the films due to exposure to ambient contaminants (**Figure S2**a, b). The absence of these contaminants in the bulk indicates the high purity of the $(Sn,Ge)O_2$ films as a result of the clean and complete reaction between both tin and germanium precursors with $H_2O_2$ when operating within the common temperature windows of both ALD processes.

The X-ray diffraction pattern of $(Sn,Ge)O_2$ films deposited on 1 inch × 1 inch quartz substrates exhibits no specific peaks from the film, which suggests nearly amorphous or nano-crystalline structure of the film.

The carrier mobility, electron carrier density and resistivity are plotted as a function of the Ge/(Ge+Sn) ratio in **Figure 1**a. Hall measurements demonstrate that the $(Sn,Ge)O_2$ films have n-type conductivities with electron concentrations tunable between $10^{18}$ $cm^{-3}$ and $10^{20}$ $cm^{-3}$. The electron Hall mobility varied only slightly with varying amount of germanium incorporation in the film which is expected as the material remains amorphous independent of germanium doping levels. The germanium doped tin oxide films showed lower carrier concentration compared to the undoped tin oxide films. Since both tin and germanium cations are in the same +4 oxidation state, we do not expect any increase in the electron concentration from germanium doping. Instead, the conductivity of $SnO_2$ films is attributed to the presence of oxygen vacancies in the material[20].

Deconvolution of the O-1s XPS spectra of $(Sn,Ge)O_2$ ALD films as presented in **Figure S3**a-c shows two components with peak centers at 531.2 eV and 532.7 eV, respectively. Neither of these photoemission lines can be assigned to O-Ge bonds as both lines exist in the O-1s region of undoped $SnO_2$, with the higher energy emission reducing in intensity as more Ge is doped into the material, in contrast to the expected behavior of the O-Ge line. Instead, the lower energy peak $O_L$ is assigned to the oxygen ions bonded to Sn ions, while the higher energy peak $O_{OV}$ can be attributed to the presence of oxygen vacancies in the $SnO_2$ sublattice. As the Ge content of the film is increased from 0 to 14 at. %, the $O_{OV}$ peak assigned to oxygen vacancies reduced from 59 % in the undoped $SnO_2$ film to 2 % in the film with 14 at. % of germanium, corresponding to a significant reduction in the concentration of oxygen vacancies. This is explained by the bond strength of Ge-O (657.5 kJ $mol^{-1}$) which is greater than that of Sn-O (528 kJ $mol^{-1}$), making it more effective at capturing oxygen and hence suppressing the formation of oxygen vacancies. The electrical conductivity of $SnO_2$ is typically attributed to the formation of oxygen vacancies, given by the equation

$$O_O^{\times} = \frac{1}{2}O_2(g) + V_O^{**} + 2e^-$$

where two electron carriers and a doubly charged oxygen vacancy are the result of the loss into the gas phase of an

oxygen unit for each $SnO_2$ unit in the material. Thus, when the germanium doping is increased, the resulting reduction in oxygen vacancies corresponds to a decrease in the electron carrier concentration of the film, giving rise to an increased electrical resistivity.

The absorption coefficient $\alpha$ is obtained from the optical transmission and reflectance measurements and calculated using

$$\alpha = \frac{1}{d}\ln\left(\frac{1-R}{T}\right)$$

where $d$ is the film thickness, $R$ and $T$ are the reflectance and transmittance of the film, respectively. The optical bandgap energy value is obtained from plots of $\alpha^2$ vs. photon energy for the various ALD films deposited on quartz substrates, using the Tauc relation for direct transitions[21]

$$\alpha(h\nu) \propto \left(h\nu - E_g\right)^{\frac{1}{2}}$$

where $\alpha(h\nu)$ is the absorption coefficient, $h\nu$ is the photon energy, and $E_g$ is the optical bandgap. The bandgap is then obtained by extrapolating to $\alpha \cdot h\nu = 0$. Bilayer samples of 500-nm-thick SnS and 5-nm-thick $SnO_2$ with various concentrations of germanium dopants were fabricated to investigate the electronic band alignment of $(Sn,Ge)O_2$ relative to SnS. The valance band offset ($\Delta E_{VB}$) and conduction band offset ($\Delta E_{CB}$) in the SnS/$(Sn,Ge)O_2$ stack are respectively calculated using the relation

$$\Delta E_{VB} = \left(E_{Sn-3d}^{SnS/(Sn,Ge)O_2} - E_{Ge-3d}^{SnS/(Sn,Ge)O_2}\right) + \left(E_{Ge-3d}^{(Sn,Ge)O_2} - E_{VBM}^{(Sn,Ge)O_2}\right) - \left(E_{Sn-3d}^{SnS} - E_{VBM}^{SnS}\right)$$

$$\Delta E_{CB} = \left(E_{Sn-3d}^{SnS/(Sn,Ge)O_2} - E_{Ge-3d}^{SnS/(Sn,Ge)O_2}\right) + \left(E_{Ge-3d}^{(Sn,Ge)O_2} - E_{VBM}^{(Sn,Ge)O_2}\right) - \left(E_{Sn-3d}^{SnS} - E_{VBM}^{SnS}\right) + \left(E_g^{(Sn,Ge)O_2} - E_g^{SnS}\right)$$

where $E_g^{(Sn,Ge)O_2}$ and $E_g^{SnS}$ are the optical band gaps of bulk $(Sn,Ge)O_2$ and SnS, respectively[22].

Bandgap bowing is demonstrated in $(Sn,Ge)O_2$ in **Figure 1**b where the bandgap of $SnO_2$ narrows initially when germanium is added to $SnO_2$ before widening towards that of $GeO_2$ (5.8 eV[23]) to complete the bowing. When increasing the doping levels of germanium reduce the electron concentrations to under $10^{19}$ $cm^{-3}$, the decreased influence of the Burstein-Moss effect is believed to be competing with the bandgap widening, contributing to the bowing effect of the bandgap. For all values of germanium content studied, the bandgap of $(Sn,Ge)O_2$ remains above 3.5 eV, making $SnO_2$ in the entire doping range highly suitable as a window layer of solar cells by possessing excellent transparency in the AM 1.5 spectrum. **Figure 1**b shows $(Sn,Ge)O_2$ films exhibit a monotonic decrease in the valence band offsets relative to SnS, resulting in an overall monotonic increase in CBOs with increasing Ge content of the $SnO_2$ film. An almost-linear relationship is observed between the CBOs and the amount of germanium doping despite bandgap bowing. This makes it easy to tune the CBO simply by controlling the $SnO_2/GeO_2$ ALD cycle ratio.

The optimal composition of the $(Sn,Ge)O_2$ buffer layer for partnering with SnS was determined by tuning the energy band alignments at the SnS/$(Sn,Ge)O_2$ heterojunction. Devices with an active area of 0.24 $cm^2$ (**Figure 3**) were fabricated using ALD SnS absorbers with different elemental compositions of $(Sn,Ge)O_2$ buffer layers. $SnO_2$:$GeO_2$ ALD sub-cycle ratios of 59:1, 39:1, 19:1, 9:1, 3:1, and 1:1 were used to fabricate the devices, and a germanium-free $SnO_2$ buffer layer is used in the baseline device. The amount of germanium in these films for the various $SnO_2$:$GeO_2$ ALD sub-cycle ratios can be found in **Figure S1**. The undoped $SnO_2$ layer formed a type-II "cliff" structure with SnS due to having a slightly negative CBO, causing the device to suffer from increased interfacial recombination near the p-n junction. While $SnO_2$ provides beneficial passivating effects at the interface between SnS and Zn(O,S), it lacked the appropriate band alignment with SnS and resulted in non-rectifying devices when the $SnO_2$ layer exceeded several nanometers in film thickness. Since germanium has demonstrated the ability to raise the conduction band energy level of $SnO_2$, doping germanium into the film shifts the heterojunction into a type-I scenario with a positive CBO, improving the rectification and hence the performance of the device. However, as we decrease the $SnO_2/GeO_2$ ALD sub-cycle ratio and consequently incorporate too much germanium into the material, the CBO with SnS increases considerably to the point where photo-generated electrons are being impeded. Although having a $(Sn,Ge)O_2$ buffer layer with an ALD cycle ratio of 19:1 demonstrated modest J-V characteristics under illumination relative to the undoped $SnO_2$ layer, the device had a low fill factor of 25 % and displayed a lackluster PCE of 0.4 %. Decreasing the amount of germanium content by switching to a $SnO_2/GeO_2$ ALD cycle ratio of 29:1 is expected to provide improved performances with the presence of a sufficiently small conduction band spike at the heterojunction, but the actual device exhibited a poor ohmic J-V response. With a $SnO_2/GeO_2$ cycle ratio of 29:1, the electron density of $(Sn,Ge)O_2$ is higher than the film with a 19:1 cycle ratio. Doping $(Sn,Ge)O_2$ with nitrogen provided a significant recovery of the diode quality by decreasing the conductivity of the buffer layer. Nitrogen is introduced into the lattice of $(Sn,Ge)O_2$ by injecting an additional dose of purified $NH_3$ gas immediately following the water vapor dose at the end of each $GeO_2$ ALD subcycle. Nitrogen incorporation in the film serves to reduce the large electron density from $5 \times 10^{19}$ $cm^{-3}$ down an order of magnitude to $6 \times 10^{18}$ $cm^{-3}$ to compensate for the higher carrier density due to the reduction in germanium doping. Charge compensation occurs when acceptor levels that are created in the $SnO_2$ band gap neutralize the electron density due to oxygen vacancies, leading to the reduced carrier density in the material[24].

The device utilizing the nitrogen doped $(Sn,Ge)O_2$ buffer layer with an ALD sub-cycle ratio of 29:1 demonstrates the best photovoltaic performance with Jsc = 12.2 $mA/cm^2$, Voc = 0.40 V, FF = 46 %, and PCE = 2.21 %. This device has the highest reported $V_{OC}$ to date for a SnS-based solar cell. The JV-characteristics in **Figure 2** demonstrates how tuning both the carrier concentration

and band energy alignments at the heterojunction are vital to optimizing the photovoltaic device efficiencies and achieving high $V_{OC}$ performance.

In conclusion, we have demonstrated the atomic layer deposition of $(Sn,Ge)O_2$ as a buffer layer for SnS-based solar cells. Significant improvement in the $V_{OC}$ can be captured through optimization of the conduction band alignments and carrier concentration of the buffer layer, achieving a $V_{OC}$ of 0.40 V and a device efficiency of 2.21 %. Germanium doping raises the conduction band level of $SnO_2$ while reducing the electron concentration by reducing the oxygen vacancies in the film. By incorporating nitrogen into the film using ammonia gas, the carrier concentration of $(Sn,Ge)O_2$ can be reduced to match the absorber layer. Our results highlight the importance and advantages of exploiting an electrically and energetically tunable buffer material such as $(Sn,Ge)O_2$ with an adjustable conduction band energy level, enabling the CBO to be adapted to a wide range of absorber materials and surfaces, while at the same time being able to change the carrier concentration to match that of the absorber material. Furthermore, eliminating the use of zinc in the n-type partner layer avoids mid-gap defects associated with Zn diffusing out from Zn(O,S) buffer layers across the p-n junction. By simultaneously serving as a passivating layer, a diffusion barrier, and an electron transport layer with tunable band alignments and adjustable carrier concentrations to match SnS, $(Sn,Ge)O_2$ has demonstrated potential as a partner material for SnS absorber layers in solar cells.

## I. SUPPLEMENTARY MATERIAL

See supplementary material for details on the influence of ALD subcycle ratios on the film composition, XPS studies on the chemical purity of the film and on the effect of Ge doping on the hydroxyl content, cross-sectional SEM study of the solar cell device stack, optical properties of the $(Sn,Ge)O_2$ film, and optimization of $(Sn,Ge)O_2$ layer thickness in the SnS-based photovoltaic devices.

## II. ACKNOWLEDGEMENTS

This work was supported in part by the U.S. Department of Energy under contract DE-EE0005329, the Center for the Next Generation of Materials by Design, an Energy Frontier Research Center funded by the U.S. Department of Energy, Office of Science, and in part by the U.S Department of Energy, Energy Efficiency and Renewable Energy Program under contract DE-EE0006334. This work was also performed in part at the CNS, a member of the National Nanotechnology Coordinated Infrastructure Network (NNCI), which is supported by the National Science Foundation under NSF Award No. 1541959, and at Harvard's X-ray laboratory. CNS is part of Harvard University.

## III. REFERENCES

1. Sinsermsuksakul, P., J. Heo, W. Noh, A.S. Hock, and R.G. Gordon, *Atomic Layer Deposition of Tin Monosulfide Thin Films*. Advanced Energy Materials, 2011. **1**(6): p. 1116-1125.
2. Ramakrishna Reddy, K.T., N. Koteswara Reddy, and R.W. Miles, *Photovoltaic properties of SnS based solar cells*. Solar Energy Materials and Solar Cells, 2006. **90**(18-19): p. 3041-3046.
3. Ichimura, M., K. Takeuchi, Y. Ono, and E. Arai, *Electrochemical deposition of SnS thin films*. Thin Solid Films, 2000. **361-362**: p. 98-101.
4. Ortiz, A., J.C. Alonso, M. Garcia, and J. Toriz, *Tin sulphide films deposited by plasma-enhanced chemical vapour deposition*. Semiconductor Science and Technology, 1996. **11**(2): p. 243-247.
5. Koteeswara Reddy, N., Y.B. Hahn, M. Devika, H.R. Sumana, and K.R. Gunasekhar, *Temperature-dependent structural and optical properties of SnS films*. Journal of Applied Physics, 2007. **101**(9): p. 093522.
6. Niemegeers, A., M. Burgelman, and A. De Vos, *On the CdS/CuInSe2 conduction band discontinuity*. Applied Physics Letters, 1995. **67**(6): p. 843-845.
7. Sun, L., R. Haight, P. Sinsermsuksakul, S. Bok Kim, H.H. Park, and R.G. Gordon, *Band alignment of SnS/Zn(O,S) heterojunctions in SnS thin film solar cells*. Applied Physics Letters, 2013. **103**(18): p. 181904.
8. Sinsermsuksakul, P., K. Hartman, S. Bok Kim, J. Heo, L. Sun, H. Hejin Park, R. Chakraborty, T. Buonassisi, and R.G. Gordon, *Enhancing the efficiency of SnS solar cells via band-offset engineering with a zinc oxysulfide buffer layer*. Applied Physics Letters, 2013. **102**(5): p. 053901.
9. Park, H.H., R. Heasley, L. Sun, V. Steinmann, R. Jaramillo, K. Hartman, R. Chakraborty, P. Sinsermsuksakul, D. Chua, T. Buonassisi, et al., *Co-optimization of SnS absorber and Zn(O,S) buffer materials for improved solar cells*. Progress in Photovoltaics: Research and Applications, 2015. **23**(7): p. 901-908.
10. Sinsermsuksakul, P., L. Sun, S.W. Lee, H.H. Park, S.B. Kim, C. Yang, and R.G. Gordon, *Overcoming Efficiency Limitations of SnS-Based Solar Cells*. Advanced Energy Materials, 2014. **4**(15): p. 1400496.
11. Tritsaris, G.A., B.D. Malone, and E. Kaxiras, *Structural stability and electronic properties of low-index surfaces of SnS*. Journal of Applied Physics, 2014. **115**(17): p. 173702.
12. Hultqvist, A., C. Platzer-Björkman, E. Coronel, and M. Edoff, *Experimental*

*investigation of Cu(In1−x,Gax)Se2/Zn(O1−z,Sz) solar cell performance*. Solar Energy Materials and Solar Cells, 2011. **95**(2): p. 497-503.
13. Repins, I., M.A. Contreras, B. Egaas, C. DeHart, J. Scharf, C.L. Perkins, B. To, and R. Noufi, *19·9%-efficient ZnO/CdS/CuInGaSe2solar cell with 81·2% fill factor*. Progress in Photovoltaics: Research and Applications, 2008. **16**(3): p. 235-239.
14. Shin, B., O. Gunawan, Y. Zhu, N.A. Bojarczuk, S.J. Chey, and S. Guha, *Thin film solar cell with 8.4% power conversion efficiency using an earth-abundant Cu2ZnSnS4 absorber*. Progress in Photovoltaics: Research and Applications, 2013. **21**(1): p. 72-76.
15. Wang, W., M.T. Winkler, O. Gunawan, T. Gokmen, T.K. Todorov, Y. Zhu, and D.B. Mitzi, *Device Characteristics of CZTSSe Thin-Film Solar Cells with 12.6% Efficiency*. Advanced Energy Materials, 2014. **4**(7): p. 1301465.
16. Barkhouse, D.A.R., R. Haight, N. Sakai, H. Hiroi, H. Sugimoto, and D.B. Mitzi, *Cd-free buffer layer materials on Cu2ZnSn(SxSe1−x)4: Band alignments with ZnO, ZnS, and In2S3*. Applied Physics Letters, 2012. **100**(19): p. 193904.
17. Waldrop, J.R., R.W. Grant, S.P. Kowalczyk, and E.A. Kraut, *Measurement of semiconductor heterojunction band discontinuities by x-ray photoemission spectroscopy*. Journal of Vacuum Science & Technology A: Vacuum, Surfaces, and Films, 1985. **3**(3): p. 835-841.
18. Scofield, J.H., A. Duda, D. Albin, B.L. Ballard, and P.K. Predecki, *Sputtered molybdenum bilayer back contact for copper indium diselenide-based polycrystalline thin-film solar cells*. Thin Solid Films, 1995. **260**(1): p. 26-31.
19. Elam, J.W., D.A. Baker, A.J. Hryn, A.B.F. Martinson, M.J. Pellin, and J.T. Hupp, *Atomic layer deposition of tin oxide films using tetrakis(dimethylamino) tin*. Journal of Vacuum Science & Technology A, 2008. **26**(2): p. 244-252.
20. Singh, A.K., A. Janotti, M. Scheffler, and C.G. Van de Walle, *Sources of electrical conductivity in SnO2*. Phys Rev Lett, 2008. **101**(5): p. 055502.
21. Tauc, J. and A. Menth, *States in the gap*. Journal of Non-Crystalline Solids, 1972. **8-10**: p. 569-585.
22. Lee, Y.S., D. Chua, R.E. Brandt, S.C. Siah, J.V. Li, J.P. Mailoa, S.W. Lee, R.G. Gordon, and T. Buonassisi, *Atomic layer deposited gallium oxide buffer layer enables 1.2 V open-circuit voltage in cuprous oxide solar cells*. Adv Mater, 2014. **26**(27): p. 4704-10.
23. Lange, T., W. Njoroge, H. Weis, M. Beckers, and M. Wuttig, *Physical properties of thin GeO2 films produced by reactive DC magnetron sputtering*. Thin Solid Films, 2000. **365**(1): p. 82-89.
24. Suapadkorn, P., W. Rakreungdet, T. Jutarosaga, and W. Samanjit, *Nitrogen – Doped $SnO_2$ Thin Films Prepared by Direct Current Magnetron Sputtering*. Advanced Materials Research, 2013. **770**: p. 169-172.

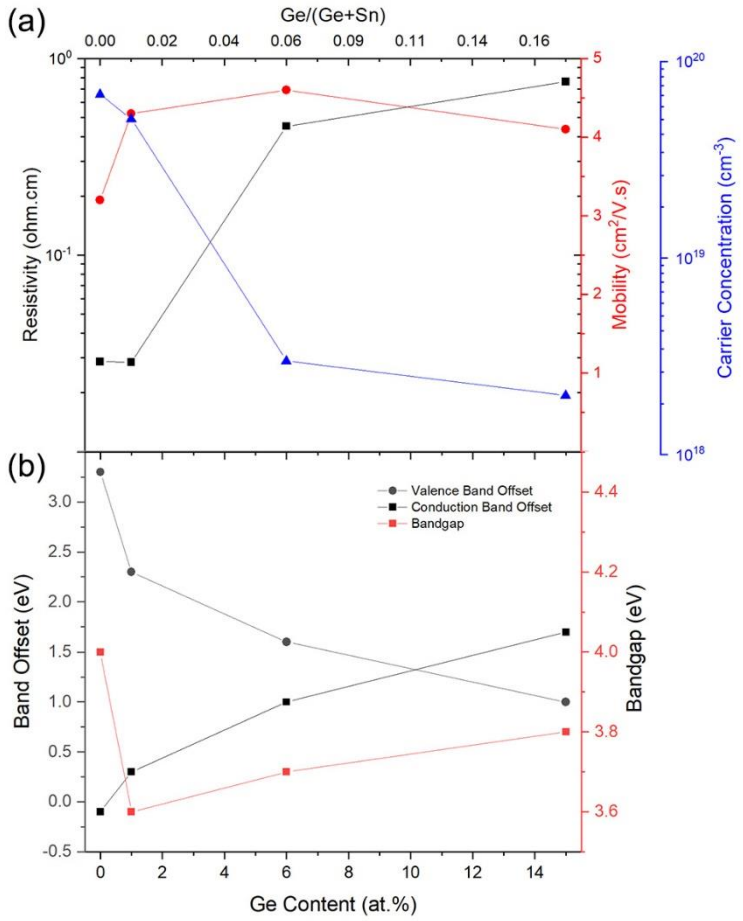


**Figure 1.** Effect of various amounts of germanium incorporation in $SnO_2$ films on (a) hall mobility, carrier concentration and resistivity, and (b) optical bandgaps as determined from absorption data and band offsets of both the valance bands and conduction bands at the heterojunction formed with SnS.

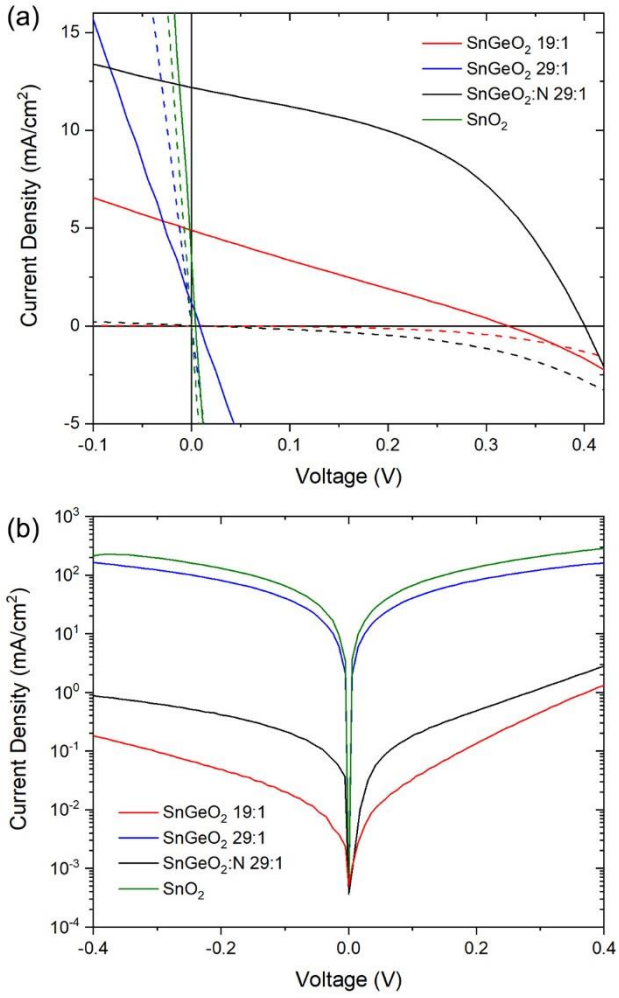


**Figure 2.** Current density-voltage characteristics of Mo (500 nm)/SnS (500 nm)/(Sn,Ge)$O_2$ (40 nm)/ZnO (10 nm)/ITO (200 nm)/Ag (500 nm) devices at various (Sn,Ge)$O_2$ compositions (a) under dark (dotted line) and AM 1.5 illumination (solid line) on a linear scale, and (b) under dark conditions on a semi-log scale.